ACS APPLIED MATERIALS & INTERFACES

Research Article

www.acsami.org

# Bottom-Up Fabrication of Activated Carbon Fiber for All-Solid-State Supercapacitor with Excellent Electrochemical Performance

Wujun Ma, Shaohua Chen, Shengyuan Yang, Wenping Chen, Wei Weng, and Meifang Zhu*

State Key Laboratory for Modification of Chemical Fibers and Polymer Materials, College of Materials Science & Engineering, Donghua University, 2999 North Renmin Road, Shanghai 201620, China

Supporting Information

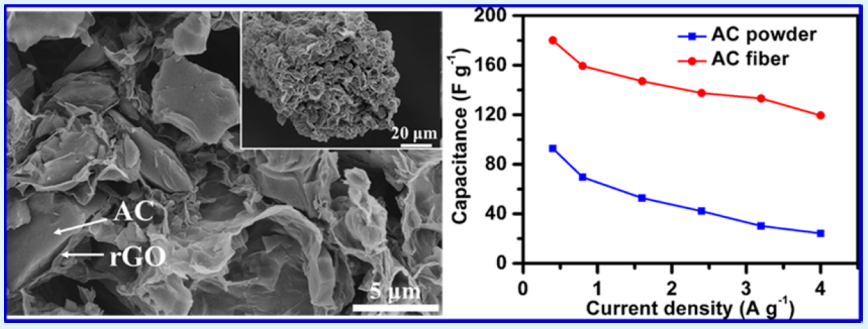


**ABSTRACT:** Activated carbon (AC) is the most extensively used electrode material for commercial electric double layer capacitors (EDLC) given its high specific surface area (SSA) and moderate cost. However, AC is primarily used in the forms of powders, which remains a big challenge in developing AC powders into continuous fibers. If AC powders can be processed into fiber, then they may be scaled up for practical applications to supercapacitors (SCs) and satisfy the rapid development of flexible electronics. Herein, we report a bottom-up method to fabricate AC fiber employing graphene oxide (GO) as both dispersant and binder. After chemical reduction, the fiber has high electrical conductivity (185 S $m^{-1}$), high specific surface area (1476.5 $m^2$ $g^{-1}$), and good mechanical flexibility. An all solid-state flexible SC was constructed using the prepared fiber as electrode, which is free of binder, conducting additive, and additional current collector. The fiber-shaped SC shows high capacitance (27.6 F $cm^{-3}$ or 43.8 F $g^{-1}$, normalized to the two-electrode volume), superior cyclability (90.4% retention after 10 000 cycles), and good bendability (96.8% retention after bending 1000 times).

**KEYWORDS:** *AC fiber, graphene oxide, wet-spinning, wearable supercapacitor, flexibility*

## INTRODUCTION

To meet the rapid advances of flexible, portable, and even wearable electronics, such as rollup displays and electronic skin, considerable efforts have been dedicated to develop corresponding energy storage and conversion systems as power sources, such as flexible supercapacitors (SCs),[1] lithium-ion batteries,[2−4] and solar cells,[5] and so on. Among these, SCs are of significant interest as energy storage devices because of their high power density, fast charge−discharge rates, long cycling life, and relatively simple configuration.[6] These advantages make SCs a favorable power source candidate in the field of flexible electronics. Recently, high-performance fiber-shaped SCs have been explored extensively to meet the growing demand for flexible and wearable electronics based on graphene fibers,[7−11] CNT fibers,[12−14] carbon fibers,[15−17] and composite fibers containing pseudocapacitive materials.[18,19] However, the relatively high cost, noncontinuous fabrication process of the fibers, and low capacitance and energy density values of the fiber-based SCs limit their practical applications.

Activated carbon (AC) with large specific surface area, relatively low cost, chemical stability, and availability is the most widely used electrode material in electric double-layer capacitors.[20] However, AC is primarily used as a powder; no research effort has been devoted to developing AC powders into continuous fibers. If AC powders can be processed into fiber, then they may be scaled up for practical applications to SCs and flexible electronics. In the chemical fiber industry, there are two main methods to fabricate fibers: melt-spinning and wet-spinning. As a result of the high-temperature stability of AC, melt-spinning is not feasible. Wet-spinning is the only viable method, as is the case for high-performance fibers such as Kevlar and Twaron fibers.[21−23] This method needs to disperse AC powders in solution at a high enough concentration suitable for effective coagulation.[24] However, as a result of their chemical inertness, the solubility of AC powders in water is poor, which hinders the direct assembly of AC powders into fiber. The most common approach to disperse insoluble materials in water is to use dispersants.[25] However, traditional

Received: April 5, 2016
Accepted: May 30, 2016
Published: May 30, 2016




DOI: 10.1021/acsami.6b04026
ACS Appl. Mater. Interfaces 2016, 8, 14622−14627

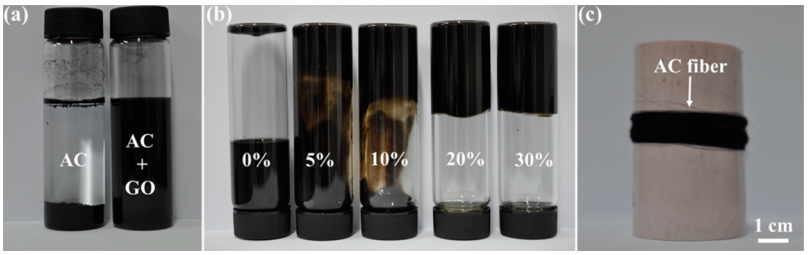


**Figure 1.** (a) Photographs of AC dispersion and GO/AC dispersion after sonication. (b) Photographs of GO/AC dispersions with different GO contents. (c) Photograph of AC fibers collected onto a bobbin.

dispersing agents such as molecular surfactants, polymers, and DNA are usually insulated, which will significantly reduce the electrochemical performance of the devices because of the increased resistivity and the addition of dead weight,[26] so the insulated dispersants need to be removed from the final fiber during coagulation or after processing, which certainly adds the complexity and cost of the fabrication process and may also deteriorate the mechanical properties of the fiber.

To address these problems, graphene oxide (GO) has been chosen as both dispersant and binder to fabricate AC fiber. We show that GO can act as an effective dispersant for AC powders and as a good binder providing both mechanical support and stability for the AC fiber. In addition, GO can be converted into highly conductive rGO through reduction, which can improve the electrical conductivity of the fiber. The fiber with large SSA, lightweight, high flexibility, and high electrical conductivity can be directly used as electrode for flexible SC. An all-solid-state fiber-shaped SC was constructed using the fiber, and it exhibited high energy and power density, robust lifetime cycling performance, and high bendability.

## EXPERIMENTAL METHODS

**Dispersion of AC Powders by GO.** Graphite oxide (GO) was prepared from flake graphite (1000 mesh, Shanghai Yifan Graphite) by a modified Hummers' method.[27] The homogeneous GO/AC (TF1B520, Shanghai Carbosino Mater., Co.) aqueous dispersions (10 mg $mL^{-1}$) at different GO/AC mass ratios, ranging from 0:100 to 30:70, were prepared by mixing AC powders and GO into distilled water, followed by sonicating for 2 h at an output power of 45 W using a digital ultrasonic processor (S-450D, Branson), then concentrated to 40 mg $mL^{-1}$ by evaporation in 60 °C water bath.

**Preparation of AC Fiber.** Continuous wet-spinning was carried out on a homemade apparatus.[8] First, homogeneous dispersion was injected into a rotating coagulation bath (acetic acid), then the resulted gel fiber was rolled onto a drum and dried at 60 °C in vacuum, and finally the fiber was reduced in an aqueous HI solution (45%, Sinopharm) at 95 °C for 12 h[28] followed by ethanol washing and drying at 60 °C for 12 h in vacuum.

**Material Characterization.** The morphology of the fibers were observed by an SU8010 field-emission scanning electron microscope (SEM, Hitachi, Japan). The resistivity was measured by a two-probe method using a PC68 high-resistance meter (Shanghai Cany Precision Instrument). Tensile strength of the fiber was measured using a XQ-1A fiber tension tester (Shanghai New Fiber Instrument). The gauge length and extension rate were 10 mm and 2 mm $min^{-1}$, respectively. Nitrogen adsorption−desorption isotherms of the fiber was measured at 77 K using Micromeritics ASAP2020. The X-ray photoelectron (XPS) spectra were obtained on an Axis Ultra DLD spectrometer (Kratos Analytical, UK) using a monochromatic Al K source.

**Electrochemical Characterization of Individual AC Fiber and AC Powder Electrodes.** The AC fiber electrode was prepared by connecting an AC fiber to stainless-steel strip end to end by silver paste. The AC powder electrode was prepared according to the reference.[29] Electrochemical tests were performed using a three-electrode configuration on an electrochemical workstation (CHI 660E) in 1 M $H_2SO_4$ electrolyte. AC fiber electrode or AC powder electrode was used as working electrode; a Pt wire and $Hg/Hg_2SO_4$ electrode were used as the counter and reference electrodes, respectively. The capacitance was calculated from GCD curves using the equation

$$C = \frac{I\Delta t}{\Delta U} \tag{1}$$

where $C$ is the total capacitance, $I$ and $\Delta t$ are the discharging current and time, respectively, and $\Delta U$ is the potential window after IR drop.

The mass capacitances ($C_M$) was calculated according to the equation

$$C_M = \frac{C}{M} \tag{2}$$

where $M$ refers to the mass of the working electrode.

**Fabrication of the Fiber-Based SCs.** The $H_3PO_4$/PVA gel electrolyte was prepared as follows: PVA (3.0 g) was added to 27.0 g of deionized water, followed by heating at 95 °C under magnetic stirring until the solution became clear. $H_3PO_4$ (3.0 g) was finally dropped to the above solution to form the gel electrolyte. To fabricate a fiber-based SCs, two fibers with the same diameter and length (1 cm) were connected to a metal wire by Ag paste, respectively, immersed in the $H_3PO_4$−PVA gel solution for 24 h, dried at room temperature until the gel electrolyte solidified, and then carefully twisted together to produce a fiber-based SC.

The electrochemical performances of the fiber-based SC were evaluated using a two-electrode configuration on an electrochemical workstation (CHI 660E). The capacitance of the supercapacitor was calculated from its discharge curves using

$$C = \frac{I\Delta t}{\Delta U} \tag{3}$$

where $C$ is the total capacitance, $I$ and $\Delta t$ are the discharging current and time, respectively, and $\Delta U$ is the potential window after IR drop.

The volumetric and mass capacitances ($C_V$ and $C_M$) of the device were calculated using the equations

$$C_V = \frac{C}{2V} \tag{4}$$

$$C_M = \frac{C}{2M} \tag{5}$$

where $V$ and $M$ refer to the volume and mass of the fiber in the single electrode, respectively. The calculation of $V$ is according to the equation

$$V = \pi R^2 L \tag{6}$$

where $R$ is the radius of the fiber and $L$ is the fiber length.

The volumetric energy ($E_V$) and power ($P_V$) density of the SCs were obtained from the equation

$$E_V = \frac{1}{2} C_V \Delta U^2 \tag{7}$$



DOI: 10.1021/acsami.6b04026
ACS Appl. Mater. Interfaces 2016, 8, 14622−14627

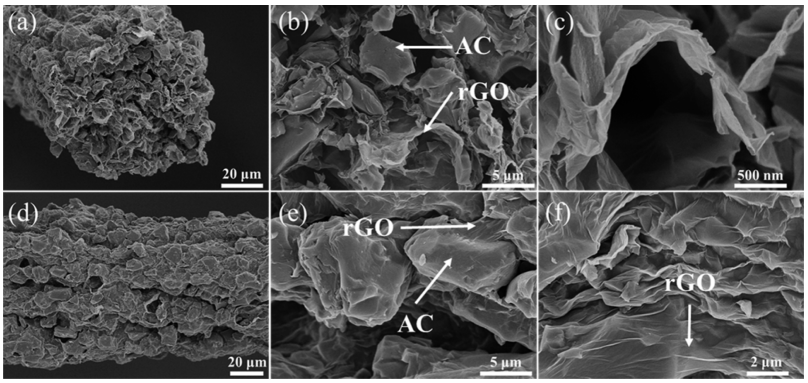


**Figure 2.** SEM images of (a–c) the cross section and (d–f) the surface of AC fiber.

$$P_V = E_V/t_{discharge} \quad (8)$$

## RESULTS AND DISCUSSION

The fabrication processes of AC fiber consist of preparation of GO/AC dispersions, wet-spinning of GO/AC fiber, and chemical reduction of GO into highly conductive rGO. First, a given amount of AC powder and GO were sonicated in deionized water. Figure 1a shows that AC powders cannot be dispersed in water even after sonication; however, with the addition of GO, the AC powders are effectively dispersed, the formed suspension is very stable, and no visible sediment was observed over 1 week, indicating that GO can well-disperse AC powders. This can be attributed to the fact that GO, with hydrophilic hydroxyl and carboxyl acid groups on the edge and unoxidized hydrophobic polyaromatic nanographene domains on the basal plane, can act as a surfactant. It can also disperse other insoluble materials such as carbon nanotubes and graphite in water.[30,31] Wet-spinning needs dispersion at a high concentration; solvent evaporation is an effective method to obtain dispersions with high concentrations. Using this procedure, we obtained GO/AC dispersions with a concentration of 40 mg $mL^{-1}$, and the contents of GO with respect to AC range from 0 to 30 wt %. Figure 1b shows that the viscosity of the pure AC solution was almost that of pure water and that the viscosity of GO/AC solutions were increasing with the content of GO. When the content of GO was above 20 wt %, a GO/AC hydrogel was formed. In contrast, no hydrogels were produced when the content was below 20 wt %. We fabricated GO/AC fiber through a wet-spinning method reported previously.[18] However, continuous GO/AC fiber cannot be obtained when the content of GO is below 30 wt % because the amount of GO was not enough to form efficient connections between adjacent AC powders. When the GO content reached 30 wt %, hundreds of meters long GO/AC fiber can be obtained (Figure 1c). Finally, to increase the conductivity of the fiber, GO were converted into highly conductive rGO through chemical reduction. XPS analysis indicates that most of the oxygenated functional groups of GO have been removed (Figure S1), and the insulated GO was converted into highly conductive rGO. As a result, the AC fiber has an electrical conductivity of 185 S $m^{-1}$ (Figure S2).

The morphology and microstructure of the as prepared AC fiber were investigated by SEM in Figure 2. Figure 2a indicates that the fiber has a circular cross section, and the diameter is about 70 $\mu$m. Within the AC fiber, the rGO layers interconnect each other and align along the axial direction, which provides a conductive network for electronic transport. Also, there are many voids clearly observed in the fiber, which can facilitate the fast ion transportation in the fiber (Figure 2a–c). The SEM images in Figure 2d–f indicate that the AC powders are homogeneously encapsulated by the rGO sheets; the rGO sheets in the fiber can act as a binder to support and connect adjacent AC powders and keep the integrity and mechanical stability of the fiber through noncovalent interactions such as van der Waals and $\pi-\pi$ interaction between rGO sheets and AC powders.[32] As a result, the fiber has a tensile strength of 22.7 MPa at 3.5% ultimate elongation (Figure S3), which is much better than that of graphene aerogel fibers fabricated by wet-spinning process.[33]

The porous structure of the AC powders and AC fiber were investigated by nitrogen adsorption–desorption measurements (Figure 3). The adsorption–desorption isotherm curve of AC

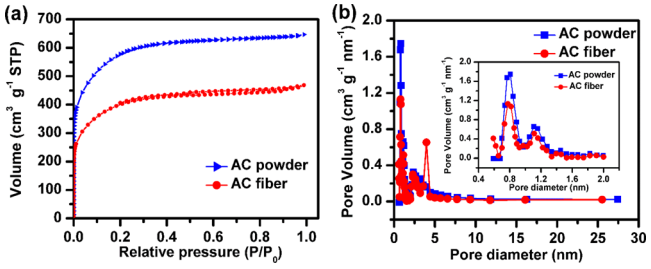


**Figure 3.** (a) Nitrogen adsorption–desorption isotherms and (b) pore size distribution of AC powder and AC fiber (inset shows the magnified pore distributions in the micropore regions).

powders (Figure 3a) is type I with no hysteresis loop, which reflects the fact that no mesopores exist in the AC powders.[34] The SSA of AC powders was determined to be 1831 $m^2$ $g^{-1}$. For AC fiber, an inconspicuous hysteresis loop could be observed in the $P/P_0$ range of 0.5–1.0, indicating the presence of mesopores, which are further identified in the pore distribution (Figure 3b). The SSA of AC fiber is 1476.5 $m^2$ $g^{-1}$, which is slightly smaller than that of AC powders. The reduced SSA of AC fiber could be attributed to the formed mesopores and macropores. The pore size distribution is shown in Figure 3b. For the AC powders, the pore diameters are predominantly in microporous range, and the mesopore volumes can be negligible. However, for the AC fiber, it possesses micropores with distributions similar to that of AC and a portion of mesopores.

The as-prepared AC fiber with high electrical conductivity and mechanical strength can be directly adhered to a stainless steel strip and used as a fiber electrode for SC; no other


DOI: 10.1021/acsami.6b04026
ACS Appl. Mater. Interfaces 2016, 8, 14622–14627

polymer binder, conducting additive, or additional current collector is needed. In the contrasting device, AC powder electrode was prepared by mixing 85 wt % AC powders, 10 wt % carbon black, and 5 wt % PTFE. We first tested the electrochemical performances of the AC powder and AC fiber electrodes in a three-electrode cell. Figure 4a shows the CV

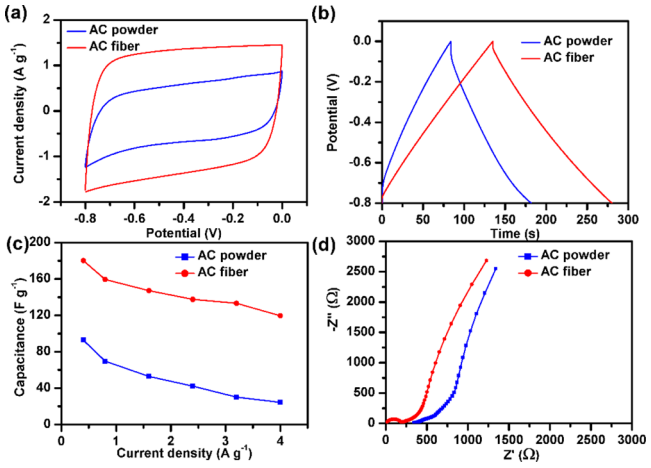


**Figure 4.** Electrochemical performance of the AC powder and AC fiber in 1 M $H_2SO_4$. (a) CV curves at a scan rate of 10 mV $s^{-1}$. (b) GCD curves at a current density of 0.8 A $g^{-1}$. (c) Specific capacitance at different current density. (d) Nyquist plots of the SCs.

curves of AC powder and AC fiber at the scan rate of 10 mV $s^{-1}$, and both of the curves are in rectangular shape, indicating ideal capacitive behavior. The CV curve of AC powder based SC exhibits a smaller area and a larger distortion, indicating that the AC fiber based SC has a much larger specific capacitance and better rate capability than does the AC powder based SC.

The GCD curve of AC powder-based SC shows a larger IR drop than does AC fiber SC (Figure 4b), indicating that the rGO sheets with higher conductivity can decrease the internal resistance of the AC fiber-based SC, which can be supported by the result of electrochemical impedance spectroscopic (EIS) (Figure 4d). The largest specific capacitance of the AC fiber is ~180.1 F $g^{-1}$ (113.8 F $cm^{-3}$) at a current density of 0.4 A $g^{-1}$. When the current density is increased from 0.4 to 4 A $g^{-1}$, the SC exhibits a high rate performance (~119.5 $g^{-1}$ at 4 A $g^{-1}$, 66.4% retention). In contrast to AC fiber, the capacitance of the AC powder SC shows fast fading as the current density increases. The capacitance values are 92.8 and 24.3 F $g^{-1}$ at a current density of 0.4 and 4 A $g^{-1}$, respectively (26.2% retention) (Figure 4c). This is mainly due to the fact that large amounts of micropores of AC powders cannot be accessed by electrolyte ions. However, with the addition of rGO, mesopores and macropores were formed in the fiber that facilitate more accessible surface area for the electrolyte ions and fast ion transportation in the electrode. Furthermore, the interconnected rGO network in the fiber increased the electrical conductivity of the fiber, reducing the internal resistance of the fiber-based SC. The outstanding electrochemical performances of the AC fiber make it a promising candidate as freestanding electrode for all-solid-state fiber-shaped SCs.

A flexible all-solid-state SC was constructed by twisting two AC fiber electrodes with poly(vinyl alcohol)−$H_3PO_4$ gel electrolyte. The electrochemical performances of the device were analyzed by a two-electrode configuration. The CV curves of the device show a quasi-rectangular shape at low scan rates (Figure 5a), and its GCD curves in Figure 5b are near triangular with low potential drop at low current densities, indicating good charge propagation across the fiber electrodes. On the basis of the calculations from GCD curves, the device exhibits a specific capacitance of 27.6 F $cm^{-3}$ at 13 mA $cm^{-3}$ and 20.2 F $cm^{-3}$ at 520 mA $cm^{-3}$ (normalized to the two-electrode volume), corresponding to mass capacitance of 43.8 and 32.1 F $g^{-1}$, respectively, outperforming many previously reported carbon-based SCs (Table S1). The cyclic stability of the SC was explored by a galvanostatic charge−discharge test. The capacitance still remained at 90.4% of its initial capacitance after 10 000 cycles, demonstrating its excellent electrochemical stability (Figure 5d). To demonstrate the flexibility of our device, it was subjected to mechanical bending under different bending angles and cycles. As shown in Figure 5e,f, there is no significant difference between the CV curves under different bending angles, and negligible change is observed between GCD curves after different bending cycles, suggesting the highly flexible property of the AC fiber based SC.

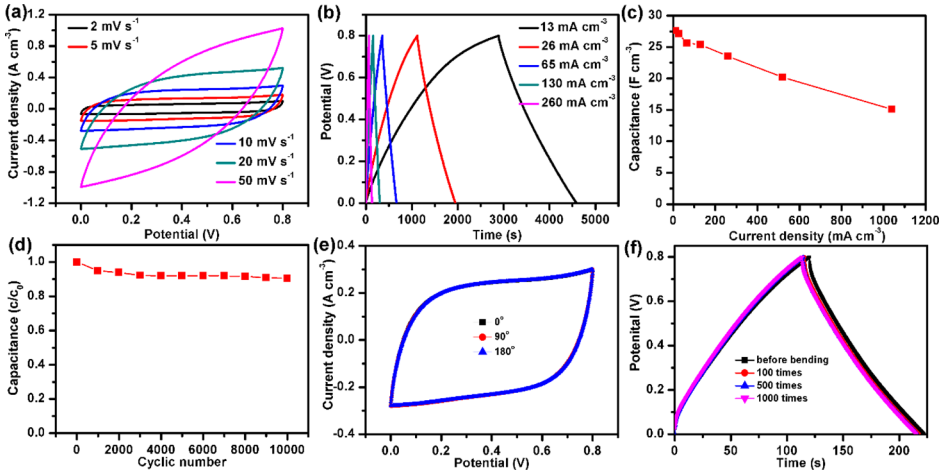


**Figure 5.** Electrochemical performances of the AC fiber-based all-solid-state SC. (a and b) CV and GCD curves. (c) Specific capacitance at various current densities. (d) Cycling performance of the SC at 520 mA $cm^{-3}$. (e) CV curves bended with different angles. (f) GCD curves before and after bending for 100, 500, and 1000 cycles.



DOI: 10.1021/acsami.6b04026
ACS Appl. Mater. Interfaces 2016, 8, 14622−14627

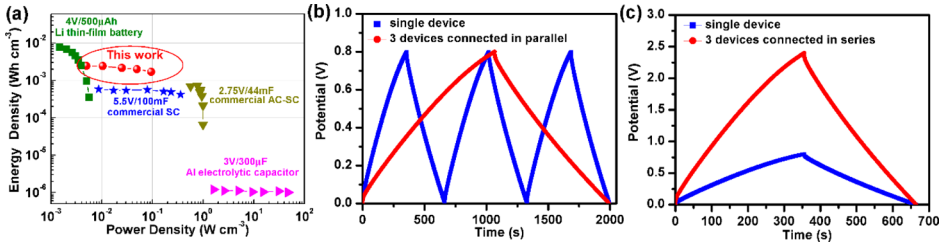


**Figure 6.** (a) Energy and power densities of the device compared with those of commercially available energy-storage systems. (b and c) GCD curves of a single device and three devices connected in parallel (b) and series (c).

The Ragone plots in Figure 6a show that the maximum energy density of our SC is up to 2.5 mWh $cm^{-3}$ (3.96 mWh $g^{-1}$) at a power density of 5 mW $cm^{-3}$, which is superior to those of commercially available SCs.[35,36] Compared with a Li thin-film battery, the SC exhibits significantly higher power densities and holds comparable energy densities.[37] This value is also higher than that of recently reported fiber-shaped supercapacitors (Table S1). For practical applications, it is usually necessary to connect SCs in series or parallel because of a limited working potential window and energy storage capacity for a single device. Compared with a single SC, the discharge time of the three SCs connected in parallel is three times that of a single SC when operated at the same current density (Figure 6b). As shown in Figure 6c, with similar discharge time, the potential window is extended from 0.8 to 2.4 V by connecting three SCs in series.

## CONCLUSIONS

We developed a bottom-up approach to fabricate AC fiber from AC powders employing GO as both dispersant and binder. The fiber has large SSA, light weight, high flexibility, and high electrical conductivity. An all-solid-state flexible SC was constructed using the as prepared AC fiber. The device exhibited high energy and power density, excellent cycling stability, and good bendability. In addition, this strategy presented here can be extended to develop other insoluble nanomaterials into fiber format, which may be promising for next-generation flexible energy storage devices.

## ASSOCIATED CONTENT

### Supporting Information

The Supporting Information is available free of charge on the ACS Publications website at DOI: 10.1021/acsami.6b04026.

XPS spectra of AC/GO fiber and AC/rGO fiber, IV curve of AC fiber measured by two-probe method, typical stress−strain curve of AC fiber, CV curves of AC fiber at different scan rates in 1 M $H_2SO_4$ measured in three-electrode cell, GCD curves of AC fiber at different current densities in 1 M $H_2SO_4$ measured in three-electrode cell, comparison of the specific capacitance and energy density of solid-state fiber supercapacitors. (PDF)

## AUTHOR INFORMATION

### Corresponding Author

*E-mail: zhumf@dhu.edu.cn.

### Notes

The authors declare no competing financial interest.

## ACKNOWLEDGMENTS

We acknowledge the financial supports from Natural Science Foundation of China (51273040) and National Natural Science Foundation for Distinguished Young Scholar of China (50925312).

## REFERENCES

(1) Yang, P.; Mai, W. Flexible Solid-State Electrochemical Supercapacitors. *Nano Energy* **2014**, *8*, 274−290.
(2) Lin, H.; Weng, W.; Ren, J.; Qiu, L.; Zhang, Z.; Chen, P.; Chen, X.; Deng, J.; Wang, Y.; Peng, H. Twisted Aligned Carbon Nanotube/Silicon Composite Fiber Anode for Flexible Wire-Shaped Lithium-Ion Battery. *Adv. Mater.* **2014**, *26*, 1217−1222.
(3) Zhou, G.; Li, F.; Cheng, H.-M. Progress in Flexible Lithium Batteries and Future Prospects. *Energy Environ. Sci.* **2014**, *7*, 1307−1338.
(4) Li, N.; Chen, Z.; Ren, W.; Li, F.; Cheng, H.-M. Flexible Graphene-based Lithium Ion Batteries with Ultrafast Charge and Discharge Rates. *Proc. Natl. Acad. Sci. U. S. A.* **2012**, *109*, 17360−17365.
(5) Fang, X.; Yang, Z.; Qiu, L.; Sun, H.; Pan, S.; Deng, J.; Luo, Y.; Peng, H. Core-Sheath Carbon Nanostructured Fibers for Efficient Wire-Shaped Dye-Sensitized Solar Cells. *Adv. Mater.* **2014**, *26*, 1694−1698.
(6) Sun, Y.; Wu, Q.; Shi, G. Graphene Based New Energy Materials. *Energy Environ. Sci.* **2011**, *4*, 1113−1132.
(7) Yu, D.; Goh, K.; Wang, H.; Wei, L.; Jiang, W.; Zhang, Q.; Dai, L.; Chen, Y. Scalable Synthesis of Hierarchically Structured Carbon Nanotube-Graphene Fibres for Capacitive Energy Storage. *Nat. Nanotechnol.* **2014**, *9*, 555−562.
(8) Chen, S.; Ma, W.; Cheng, Y.; Weng, Z.; Sun, B.; Wang, L.; Chen, W.; Li, F.; Zhu, M.; Cheng, H.-M. Scalable Non-Liquid-Crystal Spinning of Locally Aligned Graphene Fibers for High-Performance Wearable Supercapacitors. *Nano Energy* **2015**, *15*, 642−653.
(9) Kou, L.; Huang, T.; Zheng, B.; Han, Y.; Zhao, X.; Gopalsamy, K.; Sun, H.; Gao, C. Coaxial Wet-Spun Yarn Supercapacitors for High-Energy Density and Safe Wearable Electronics. *Nat. Commun.* **2014**, *5*, 3754.
(10) Meng, Y. N.; Zhao, Y.; Hu, C. G.; Cheng, H. H.; Hu, Y.; Zhang, Z. P.; Shi, G. Q.; Qu, L. T. All-Graphene Core-Sheath Microfibers for All-Solid-State, Stretchable Fibriform Supercapacitors and Wearable Electronic Textiles. *Adv. Mater.* **2013**, *25*, 2326−2331.
(11) Huang, G.; Hou, C.; Shao, Y.; Zhu, B.; Jia, B.; Wang, H.; Zhang, Q.; Li, Y. High-Performance All-Solid-State Yarn Supercapacitors Based on Porous Graphene Ribbons. *Nano Energy* **2015**, *12*, 26−32.
(12) Ren, J.; Li, L.; Chen, C.; Chen, X. L.; Cai, Z. B.; Qiu, L. B.; Wang, Y. G.; Zhu, X. R.; Peng, H. S. Twisting Carbon Nanotube Fibers for Both Wire-Shaped Micro-Supercapacitor and Micro-Battery. *Adv. Mater.* **2013**, *25*, 1155−1159.
(13) Ren, J.; Bai, W. Y.; Guan, G. Z.; Zhang, Y.; Peng, H. S. Flexible and Weaveable Capacitor Wire Based on a Carbon Nanocomposite Fiber. *Adv. Mater.* **2013**, *25*, 5965−5970.
(14) Sun, H.; You, X.; Deng, J. E.; Chen, X. L.; Yang, Z. B.; Ren, J.; Peng, H. S. Novel Graphene/Carbon Nanotube Composite Fibers for


DOI: 10.1021/acsami.6b04026
ACS Appl. Mater. Interfaces 2016, 8, 14622−14627

Efficient Wire-Shaped Miniature Energy Devices. *Adv. Mater.* **2014**, *26*, 2868−2873.
(15) Xiao, X.; Li, T.; Yang, P.; Gao, Y.; Jin, H.; Ni, W.; Zhan, W.; Zhang, X.; Cao, Y.; Zhong, J.; Gong, L.; Yen, W.-C.; Mai, W.; Chen, J.; Huo, K.; Chueh, Y.-L.; Wang, Z. L.; Zhou, J. Fiber-Based All-Solid-State Flexible Supercapacitors for Self-Powered Systems. *ACS Nano* **2012**, *6*, 9200−9206.
(16) Yuan, L.; Lu, X.-H.; Xiao, X.; Zhai, T.; Dai, J.; Zhang, F.; Hu, B.; Wang, X.; Gong, L.; Chen, J.; Hu, C.; Tong, Y.; Zhou, J.; Wang, Z. L. Flexible Solid-State Supercapacitors Based on Carbon Nanoparticles/$MnO_2$ Nanorods Hybrid Structure. *ACS Nano* **2012**, *6*, 656−661.
(17) Zhang, D.; Zhang, Y.; Luo, Y.; Chu, P. K. Highly Porous Honeycomb Manganese Oxide@Carbon Fibers Core−Shell Nanocables for Flexible Supercapacitors. *Nano Energy* **2015**, *13*, 47−57.
(18) Ma, W.; Chen, S.; Yang, S.; Chen, W.; Cheng, Y.; Guo, Y.; Peng, S.; Ramakrishna, S.; Zhu, M. Hierarchical $MnO_2$ Nanowire/Graphene Hybrid Fibers with Excellent Electrochemical Performance for Flexible Solid-State Supercapacitors. *J. Power Sources* **2016**, *306*, 481−488.
(19) Sun, G.; Liu, J.; Zhang, X.; Wang, X.; Li, H.; Yu, Y.; Huang, W.; Zhang, H.; Chen, P. Fabrication of Ultralong Hybrid Microfibers from Nanosheets of Reduced Graphene Oxide and Transition-Metal Dichalcogenides and their Application as Supercapacitors. *Angew. Chem.* **2014**, *126*, 12784−12788.
(20) Sevilla, M.; Mokaya, R. Energy Storage Applications of Activated Carbons: Supercapacitors and Hydrogen Storage. *Energy Environ. Sci.* **2014**, *7*, 1250−1280.
(21) Yang, H. *Kevlar Aramid Fiber*; Wiley: Chichester, U.K., 1993; pp 200.
(22) Schuster, D.Twaron in Composites and Protective Clothing. Proceedings of Textiles and Composites '92, Tampere, Finland, June 15−18, 1992; VTT Symposium 133; VTT Technical Research Center of Finland, Textile Laboratory: Espoo, Finland, 1992; p 233.
(23) Behabtu, N.; Young, C. C.; Tsentalovich, D. E.; Kleinerman, O.; Wang, X.; Ma, A. W. K.; Bengio, E. A.; ter Waarbeek, R. F.; de Jong, J. J.; Hoogerwerf, R. E.; Fairchild, S. B.; Ferguson, J. B.; Maruyama, B.; Kono, J.; Talmon, Y.; Cohen, Y.; Otto, M. J.; Pasquali, M. Strong, Light, Multifunctional Fibers of Carbon Nanotubes with Ultrahigh Conductivity. *Science* **2013**, *339*, 182−186.
(24) Ericson, L. M.; Fan, H.; Peng, H. Q.; Davis, V. A.; Zhou, W.; Sulpizio, J.; Wang, Y. H.; Booker, R.; Vavro, J.; Guthy, C.; Parra-Vasquez, A. N. G.; Kim, M. J.; Ramesh, S.; Saini, R. K.; Kittrell, C.; Lavin, G.; Schmidt, H.; Adams, W. W.; Billups, W. E.; Pasquali, M.; Hwang, W. F.; Hauge, R. H.; Fischer, J. E.; Smalley, R. E. Macroscopic, Neat, Single-Walled Carbon Nanotube Fibers. *Science* **2004**, *305*, 1447−1450.
(25) Barisci, J. N.; Tahhan, M.; Wallace, G. G.; Badaire, S.; Vaugien, T.; Maugey, M.; Poulin, P. Properties of Carbon Nanotube Fibers Spun from DNA-Stabilized Dispersions. *Adv. Funct. Mater.* **2004**, *14*, 133−138.
(26) Presser, V.; Zhang, L.; Niu, J. J.; McDonough, J.; Perez, C.; Fong, H.; Gogotsi, Y. Flexible Nano-felts of Carbide-Derived Carbon with Ultra-high Power Handling Capability. *Adv. Energy Mater.* **2011**, *1*, 423−430.
(27) Hummers, W. S.; Offeman, R. E. Preparation of Graphitic Oxide. *J. Am. Chem. Soc.* **1958**, *80*, 1339−1339.
(28) Pei, S.; Zhao, J.; Du, J.; Ren, W.; Cheng, H.-M. Direct Reduction of Graphene Oxide Films into Highly Conductive and Flexible Graphene Films by Hydrohalic Acids. *Carbon* **2010**, *48*, 4466−4474.
(29) Zhou, Q.; Gao, J.; Li, C.; Chen, J.; Shi, G. Composite Organogels of Graphene and Activated Carbon for Electrochemical Capacitors. *J. Mater. Chem. A* **2013**, *1*, 9196−9201.
(30) Qiu, L.; Yang, X.; Gou, X.; Yang, W.; Ma, Z.-F.; Wallace, G. G.; Li, D. Dispersing Carbon Nanotubes with Graphene Oxide in Water and Synergistic Effects between Graphene Derivatives. *Chem. - Eur. J.* **2010**, *16*, 10653−10658.
(31) Cote, L. J.; Kim, J.; Tung, V. C.; Luo, J.; Kim, F.; Huang, J. Graphene Oxide as Surfactant Sheets. *Pure Appl. Chem.* **2010**, *83*, 95.
(32) Kim, J.; Cote, L. J.; Kim, F.; Yuan, W.; Shull, K. R.; Huang, J. Graphene Oxide Sheets at Interfaces. *J. Am. Chem. Soc.* **2010**, *132*, 8180−8186.
(33) Xu, Z.; Zhang, Y.; Li, P. G.; Gao, C. Strong, Conductive, Lightweight, Neat Graphene Aerogel Fibers with Aligned Pores. *ACS Nano* **2012**, *6*, 7103−7113.
(34) Li, X.; Zang, X.; Li, Z.; Li, X.; Li, P.; Sun, P.; Lee, X.; Zhang, R.; Huang, Z.; Wang, K.; Wu, D.; Kang, F.; Zhu, H. Large-Area Flexible Core−Shell Graphene/Porous Carbon Woven Fabric Films for Fiber Supercapacitor Electrodes. *Adv. Funct. Mater.* **2013**, *38*, 4862−4869.
(35) El-Kady, M. F.; Kaner, R. B. Scalable Fabrication of High-Power Graphene Micro-Supercapacitors for Flexible and On-Chip Energy Storage. *Nat. Commun.* **2013**, *4*, 1475.
(36) El-Kady, M. F.; Strong, V.; Dubin, S.; Kaner, R. B. Laser Scribing of High-Performance and Flexible Graphene-Based Electrochemical Capacitors. *Science* **2012**, *335*, 1326−1330.
(37) Pech, D.; Brunet, M.; Durou, H.; Huang, P.; Mochalin, V.; Gogotsi, Y.; Taberna, P.-L.; Simon, P. Ultrahigh-Power Micrometre-Sized Supercapacitors Based on Onion-Like Carbon. *Nat. Nanotechnol.* **2010**, *5*, 651−654.


DOI: 10.1021/acsami.6b04026
*ACS Appl. Mater. Interfaces* 2016, 8, 14622−14627